Theory and Demonstration of Narrowband Bent Hairpin Filters Integrated With AC-Coupled Plasma Limiter Elements

Lee W. Cross, *Student Member, IEEE*, Mohammad J. Almalkawi, *Member, IEEE*, and Vijay K. Devabhaktuni, *Senior Member, IEEE*

***Abstract*—A novel narrowband filter with integral high-power microwave limiter behavior is proposed to protect cost-sensitive microwave systems. The filter-limiter consists of a third-order microstrip bent hairpin filter with encapsulated gas plasma limiters, designed for operation at 870 MHz. An equivalent circuit model is presented for the ac-coupled plasma-shell components used in this study, and parameter values were extracted from measured results and electromagnetic simulation. The theory of operation of the proposed filter-limiter was experimentally validated and key predictions were demonstrated including two modes of operation in the on-state: a constant output power mode and constant attenuation mode at relatively higher power. The filter-limiter operates passively from incident microwave energy, and can also use an external priming voltage source to reduce the limiter turn-on power threshold and reduce output power variation during limiting.**

***Index Terms*—Bandpass filter, bent hairpin, microstrip filter, plasma limiter.**

I. Introduction

MICROWAVE communication systems are susceptible to damage from high-power microwave (HPM) energy. While military systems are hardened against this threat, many civilian electronic systems are designed to meet only modest immunity requirements and remain unprotected. Consequently, many public and private electronic systems are vulnerable to damage from accidental exposure to high-power radars or deliberate attack by terrorists [1]. HPM energy couples into systems through intended signal paths such as antennas and sensors, known as front-door coupling, and unintended entry points such as enclosure slots and wire harnesses, called back-door coupling. This study is concerned with the former case that may be addressed by rejecting out-of-band energy (i.e., filtering) and limiting in-band energy.

Typically, limiters are located between the antenna and sensitive RF components, and are often composed of multiple stages to meet protection specifications [2]. Civilian communication systems usually have severe cost constraints and cannot tolerate performance degradation caused by traditional limiter technologies. Novel limiter technologies are sought to address protection and cost concerns.

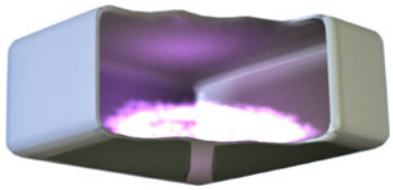

Fig. 1. Plasma-shell cross-sectional view showing plasma across two electrodes.

Commonly used diode limiters are usually the final stage of protection and can operate over many octaves of bandwidth [3], but impose significant insertion loss especially with multiple diode stages and often require additional limiter technologies to handle high-power levels [4]. Plasma limiters provide protection up to the highest power levels, and are composed of bulky gas-filled waveguides with discharge gaps located at maximum electric (E)-field points [5], or more compact transverse electromagnetic (TEM) mode structures with field-enhancing features [6]. Operational life is limited by the direct contact of intense plasma that erodes electrodes and contaminates or entraps the fill gas [7]. Other limiter technologies use thin films with rapidly changing electrical properties [8], and superconductor limiters are mentioned for completeness [9]. Therefore, the objective of this research is to utilize discrete plasma limiter components as HPM protection elements in a traditional bandpass filter structure. This creates a novel HPM protection solution for cost-sensitive communication systems with narrowband filters such as RF preselect filters [10]. These filters are composed of one or more narrowband bandpass filters designed to reject unwanted frequency bands from the RF path ahead of sensitive active circuits.

Plasma components used in this study are referred to as plasma-shells that consist of a hollow, hermetic shell of any shape encapsulating a controlled-pressure gas that can be ionized into conductive plasma, as shown in Fig. 1. The thin shell material used in this study is alumina, a strong and lightweight ceramic with exceptionally low loss, making plasma-shells nearly lossless components when inactive.

Manuscript received December 9, 2012; revised February 5, 2013; accepted February 12, 2013. This work was supported in part by the National Science Foundation EDI Award 1000744.

The authors are with the Electrical Engineering and Computer Science Department, University of Toledo, Toledo, OH 43606 USA (e-mail: lcross@teamist.com; malmalk@rockets.utoledo.edu; Mohammad.Almalkawi@utoledo.edu; Vijay.Devabhaktuni@utoledo.edu).

Color versions of one or more of the figures in this paper are available online at http://ieeexplore.ieee.org.

Digital Object Identifier 10.1109/TEMC.2013.2247403

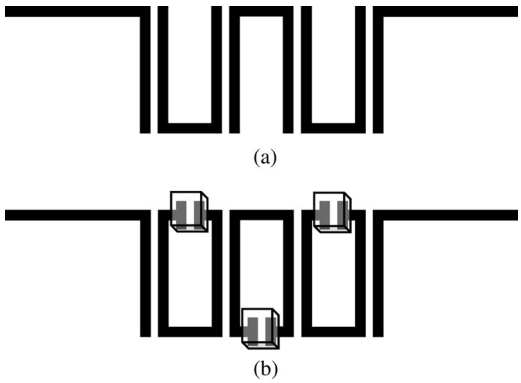

Fig. 2. (a) Traditional microstrip bent hairpin filter and (b) proposed plasma filter-limiter with encapsulated plasma devices placed at maximum E-field locations.

Conductive electrodes are patterned on one or more sides of the shell to apply an electric field of sufficient intensity to excite the interior gas into plasma. Impedance across the electrodes changes dramatically with the degree of plasma ionization [11] and allows the plasma-shell to be used as a switchable element.

Plasma-shells provide long life and operation at extreme temperatures because they are ac-coupled devices where the electrodes are protected from direct contact with plasma by the refractory dielectric shell, eliminating electrode erosion and gas contamination unlike conventional dc-coupled plasma devices that have typical service life measured in several thousands of hours [12].

To prove the concept in low-cost planar form, the structure is derived from a microstrip bent hairpin filter, shown in Fig. 2(a), because of its compact size and good electrical performance [13]. Higher Q-factor is attainable using more complicated 3-D structures. Plasma-shells are placed across the ends of each $\lambda/2$ resonator as shown in Fig. 2(b) in which there is high E-field gradient at resonance. The combined filter-limiter acts as a bandpass filter in the off-state (i.e., without plasma) and as a high-power limiter in the on-state (i.e., with plasma). It is worth mentioning that this series-connected configuration provides twice the voltage across plasma-shells versus a grounded $\lambda/4$ resonator with shunt-connected plasma-shells, reducing turn-on power threshold and activation time. For an optimal filter design, voltage across plasma-shells should be maximized by increasing resonator characteristic impedance, which must be balanced with decreasing Q-factor.

Although the resonator structure looks similar to the square open-loop resonator, it is more closely related to the bent hairpin filter because the primary design motivations are area reduction and maximized E-field, rather than easily accomplished cross-coupled filter topologies [14], [15]. Cross coupling with plasma limiter elements would cause an undesirable behavior—each transmission zero would create a spurious passband at high incident power levels, which may be more appropriate for a high-power multiplexer or Q-switch.

Gas plasma devices using low-pressure noble gas mixtures often exhibit relatively low conductivity, although there is much room for improvement through optimization of many variables including gas mixture, pressure, drive waveform, electrode geometry, wall material, priming methods, etc., that are beyond the scope of this study [16]. Even with low conductivity in the on-state, placing the plasma element in a resonant structure allows voltage magnification to effectively transform its impedance to a much lower value capable of considerable impedance mismatch during limiting. In the off-state, the plasma-shell has the potential for near-zero loss, minimizing impact on filter performance.

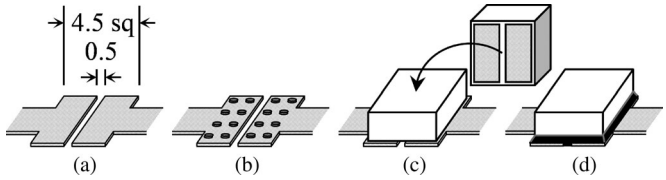

Fig. 3. Plasma-shell SMT assembly process where (a) PCB pad is (b) stenciled with conductive epoxy, then (c) shell is machine placed, and (d) high E-field gap and electrodes are sealed with underfill epoxy.

This paper is organized as follows. Section II presents ac-coupled plasma filter-limiter theory and validates it with a single resonator fixture. Section III describes the design, modeling, and measurement of a third-order filter-limiter showing good agreement in off- and on-states. Section IV summarizes the work and draws conclusions.

II. Plasma Filter-Limiter Theory

A. Plasma Element

The basic operating principle of a plasma limiter is that when forward power exceeds a turn-on threshold, a plasma discharge creates a low-impedance discontinuity that initiates on the time scale of hundreds of picoseconds to hundreds of nanoseconds. In the on-state, the plasma operates in a constant-voltage regime and limits forward power to a "clamping" value, absorbing and reflecting the remaining power. Plasma exists until forward power falls below the turn-off threshold, decaying to the off-state with a recombination time constant on the order of microseconds [17], [18].

Electrodes are the electrical interface between the internal plasma and the external circuit. Plasma-shells can be electroded in any geometry across multiple sides. Shells used in this study are electroded on one side with a 0.5 mm gap. Overall dimensions are 4.6 mm $\times$ 4.6 mm $\times$ 2.0 mm with 0.3 mm wall thickness, weighing 71 mg each. Fill gas is 0.1% argon with balance of neon, a common Penning mixture, at 240 torr [19]. Fig. 3 shows how plasma-shells are placed on printed circuit board (PCB) substrates using standard surface mount technology (SMT) processes.

B. Plasma-Shell Equivalent Circuit

The plasma-shell equivalent circuit model shown in Fig. 4 is adapted from Slottow & Bitzer's classic ac-coupled two-electrode plasma display panel (PDP) pixel equivalent circuit model [20], where electrodes apply E-field across the enclosed gas through a thin dielectric layer (i.e., the shell wall). Wall capacitance C_w is in series with gas impedance R_g, and a small

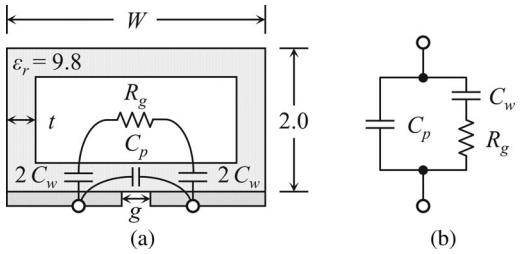

Fig. 4. Electroded plasma-shell: (a) physical structure and (b) simplified equivalent circuit model.

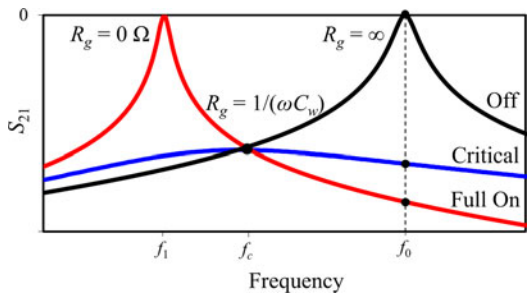

Fig. 5. First-order filter-limiter theoretical operation in off-, critical, and on-states shows high attenuation at critical gas conductivity and emergence of spurious passband at high gas conductivity.

parallel capacitance C_p accounts for the high-dielectric-constant shell in contact with electrodes. The off-state model simplifies to C_p, and the on-state model includes parallel impedance from gas that ionizes into a plasma sheet R_g in series with C_w. This simple model is sufficient to predict first-order effects caused by changes in gas impedance. Equation (1) estimates the upper bound of C_w as half the capacitance of one electrode across the shell, evaluating to 1.1 pF for shells used in this study

$$C_w \leq \frac{1}{2}\varepsilon_0\varepsilon_r \frac{(W-2t-g)/2 \times (W-2t)}{t} = 1.1 \text{ pF}. \quad (1)$$

C. First-Order Filter-Limiter

The theoretical performance of a first-order filter-limiter is shown in Fig. 5. In the off-state, the filter exhibits center frequency f_0. Insertion loss increases to nearly the maximum value as the gas ionizes and R_g approaches the critical value equal to the shell wall reactance at the critical frequency f_c.

With $R_g > 1/(\omega C_w)$, the plasma-shell acts as a lossy element that dominates the response with high insertion loss. With $R_g < 1/(\omega C_w)$, wall capacitance C_w dominates the response and a spurious passband emerges at $f_1 \ll f_0$. This is not as troublesome as it appears for several reasons: emergence of the spurious passband requires very high power levels and is well outside the filter passband, and subsequent filter-limiter stages will attenuate the spurious passband.

The filter-limiter shown in Fig. 6 was built to validate the proposed plasma-shell circuit model in its application as a filter-limiter. The design specifications are $f_0 = 880$ MHz to coincide with the center frequency of the test system amplifier power band, and a narrow bandwidth of 1% for maximum voltage across the plasma-shell. Resonator trace width was chosen to be

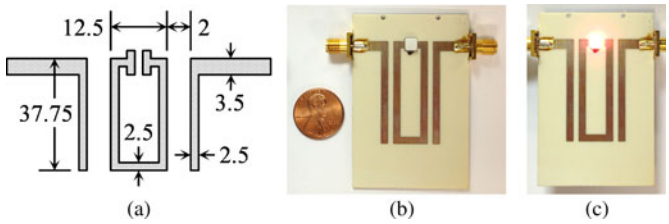

Fig. 6. First-order filter-limiter (a) layout and (b) fabricated device in off-state and (c) on-state.

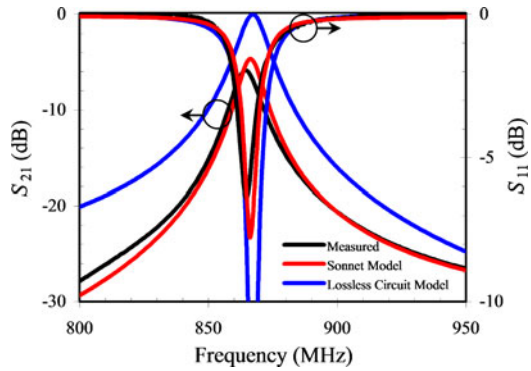

Fig. 7. First-order filter-limiter measured results compared to simulated data using Sonnet model and lossless circuit model.

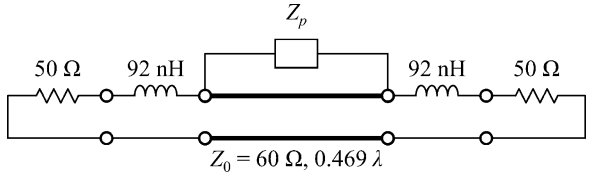

Fig. 8. First-order filter-limiter lossless distributed circuit model.

2.5 mm as a tradeoff between higher characteristic impedance Z_0 of 60 Ω and good unloaded quality factor Q_u. The magnetic coupling to the 50 Ω ports is adjusted with spacing to the resonator [21]. Filters in this study were photo-etched from Rogers 4003C with 18 μm copper-clad [22].

The filter's passband was measured with an HP 8720B vector network analyzer (VNA), first without plasma-shell measuring $f_0 = 987$ MHz, fractional bandwidth (FBW) of 1.3%, and insertion loss of 3.0 dB. Mounting the plasma-shell reduced the passband to $f_0 = 867$ MHz, with an FBW of 1.2% and an insertion loss of 4.7 dB.

Filter geometry was modeled with the aid of Sonnet EM which is based on the method of moments [23]. A lumped port was defined at the plasma-shell pad to model the plasma-shell impedance Z_p as an S-parameter component, allowing estimates of model parameters and filter performance. Fig. 7 shows good agreement between measured results, the Sonnet model with substrate parameters set to loss tangent $\delta = 0.0021$ and dielectric constant $\varepsilon_r = 3.95$, and the lossless circuit theory model in Fig. 8 optimized to match measured data.

Plasma-shell model parameter values were determined by adjusting Sonnet model parameters to match measured results.

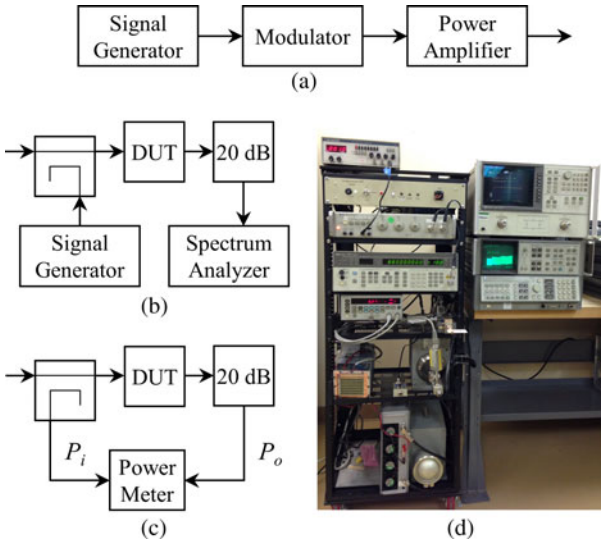

Fig. 9. High-power test setup consisting of (a) modulated power source, (b) high-dynamic-range wideband test setup, (c) limiter attenuation test setup, and (d) picture of equipment.

First, C_p was determined to be 0.33 pF by adjusting capacitance so that f_0 reduces from 987 MHz (with $C_p = 0$ pF) to 867 MHz. This uses S-parameter measurements in the off-state, and the remaining parameters were extracted from filter-limiter measured data in the on-state.

The on-state wideband response is difficult to measure because of high-power levels. The test setup in Fig. 9 isolates sensitive measurement equipment from high-power pulses. It consists of a modulated pulse source that outputs up to 54 dBm over a useful range of 820–920 MHz, and two different measurement configurations. Fig. 9(b) shows a high-dynamic-range setup that allows attenuation measurement at frequencies other than the drive frequency. The HP 8566B spectrum analyzer has a dynamic range of 125 dB (much greater than the VNA), which is necessary to measure the 15 dBm measurement signal through the 35 dB directional coupler and 20 dB attenuator, providing measurement dynamic range of 70 dB. Measurement setup frequency response is flat over 600–900 MHz. A drive pulse rate of 10 Hz with 12.5% duty cycle reduces thermal effects at high power levels. Fig. 9(c) shows a traditional limiter measurement setup that measures input and output powers with an HP 438A power meter and HP 8481A sensors.

Wideband measured results are shown in Fig. 10 as discrete data points taken at regular frequency intervals and input power increasing in decades. The next model parameter to extract is C_w, which could be directly measured from the spurious passband frequency if $R_g = 0\ \Omega$, but such high gas conductivity cannot be achieved with this setup. A realistic approach is to extract C_w from the critical point where transmission responses cross for all input power levels, located at $f_c = 775$ MHz. C_w was determined to be 0.73 pF by setting $R_g = 0\ \Omega$ in the Sonnet model and adjusting until the response intersected the critical point. The extracted value is less than that predicted by (1) likely because the plasma sheet is weekly ionized far from the electrode gap, reducing its effective area.

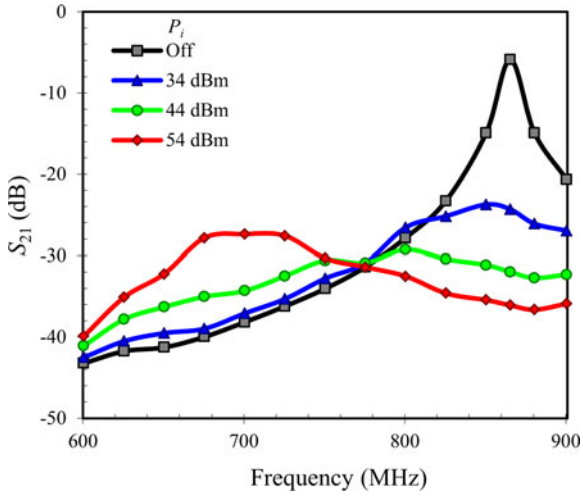

Fig. 10. First-order filter-limiter wideband results show disappearance of passband with increasing input power at f_0, and emerging spurious passband at the highest tested power level. All traces cross at the critical point at 775 MHz.

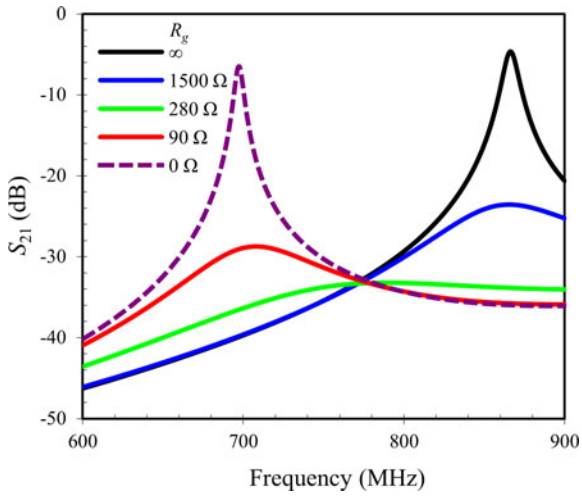

Fig. 11. Sonnet model agrees with measured results in Fig. 10 with optimized R_g values (given in legend) for each tested input power level. The Sonnet model predicts a spurious passband at 698 MHz for $R_g = 0\ \Omega$.

Finally, R_g was estimated by optimizing Sonnet model values to match measured wideband test data at each input power level. Values of R_g are given in Fig. 11 for each tested power level in Fig. 10. It is observed that the wideband response with an input power of 44 dBm matches the Sonnet EM model with R_g equal to the critical gas resistance of 280 Ω, showing a nearly flat response with peak at the critical point. The Sonnet model predicts the location of the spurious passband $f_1 = 698$ MHz (with $R_g = 0\ \Omega$).

With accurate model parameters extracted, the test setup in Fig. 9(c) was used to measure input and output powers with high-power pulses at f_0. The off-state trace in Fig. 12 shows power passing directly through the filter less insertion loss with slope of 1, and the plasma-shell self-activates at turn-on power threshold of 28 dBm, while in the on-state at low incident power, the output power is clamped to ∼8 dBm with slope of 0.14. The flat slope defines the limiter region where the plasma-shell acts

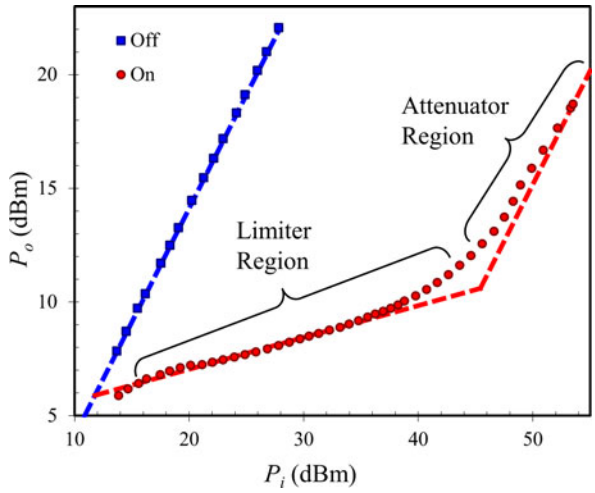

Fig. 12. First-order limiter characteristic curve in off- and on-state showing distinct limiter and attenuator operating regions.

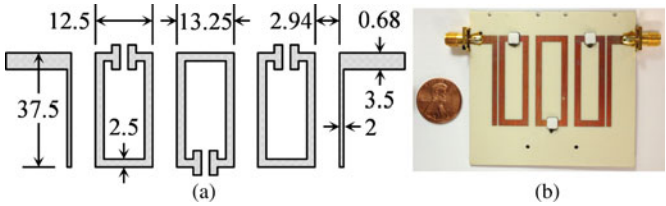

Fig. 13. Third-order filter-limiter (a) layout and (b) fabricated device.

as a constant-voltage limiter where gas conductivity modulates to hold output power constant independent of input power. The plasma-shell remains ON until input power falls below 14 dBm, showing a hysteresis region of 14 dB.

Voltage across plasma-shell terminals cannot be directly measured but can be predicted by the Sonnet model. The voltage multiplication factor is determined to be 16.8 by applying a known forward power and measuring voltage across the plasma-shell terminals. The plasma-shell turn-on threshold voltage is 133 V, calculated as the product of the filter input voltage at turn-on threshold power, voltage multiplication factor, and $\sqrt{2}$ to convert RMS to peak voltage.

At input power levels above 46 dBm, the device operates in the attenuator region where slope is 1 and the device has high fixed insertion loss independent of input power. Measurements show the slope approaching 1 at the highest tested power level. Measured attenuation at 46 dBm is 33.5 dB, similar to the value of 29.1 dB predicted by the Sonnet model with critical gas conductivity ($R_g = 280\ \Omega$). Higher attenuation can be achieved by cascading filter-limiter stages.

III. Third-Order Filter-Limiter

With plasma-shell model parameters extracted and theory validated, a filter-limiter of higher order was designed to confirm the validity of the proposed concept and to demonstrate higher attenuation in a practical structure. The filter specification is third-order bandpass response with $f_0 = 880$ MHz and FBW of 5%. The fabricated filter is shown with dimensions in Fig. 13.

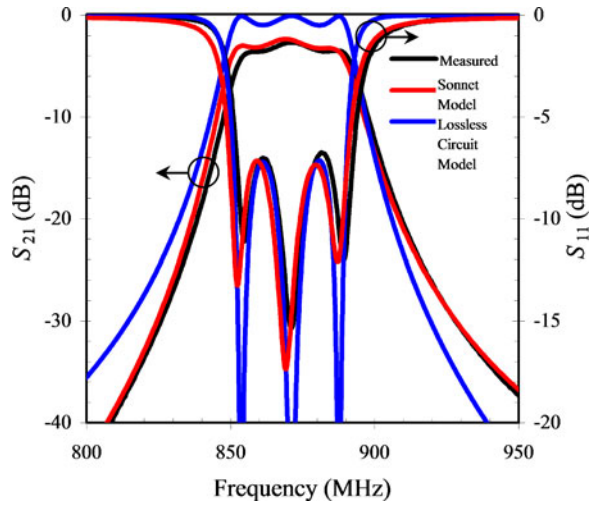

Fig. 14. Third-order filter-limiter measured results agree with the Sonnet model and circuit theory.

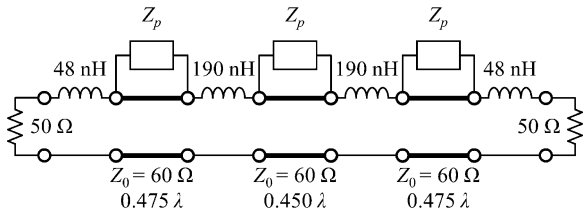

Fig. 15. Third-order filter-limiter distributed circuit model.

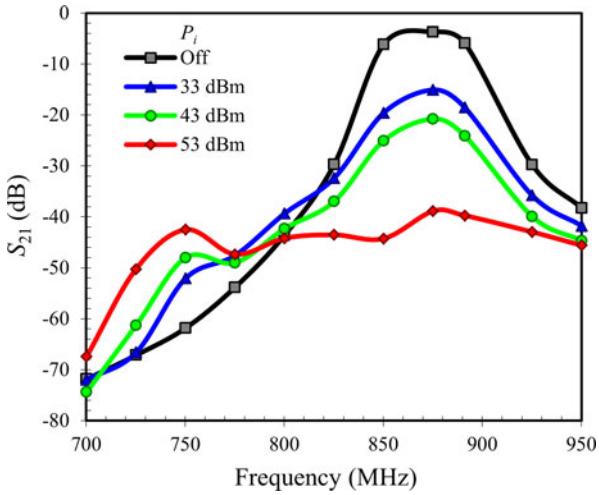

Fig. 16. Third-order filter-limiter wideband measured results show disappearance of the passband as incident power increases.

With plasma-shells mounted, the off-state measured response is shown in Fig. 14 with $f_0 = 872$ MHz, FBW of 4.9%, and insertion loss of 3.3 dB. Off-state measured results match the Sonnet model and lossless circuit model in Fig. 15.

The wideband transmission response is shown in Fig. 16, driven near the passband center at 870 MHz with increasing power levels. The passband disappears as input power increases, yielding a nearly flat response at maximum power. Attenuation increases significantly as input power increases from 43 to 53 dBm, coinciding with activation of the second plasma-shell

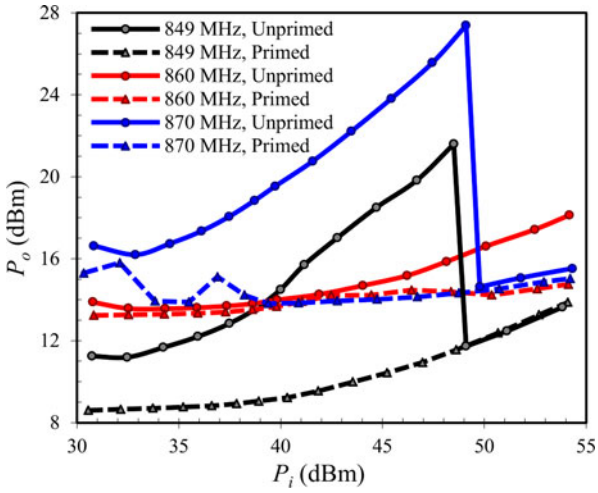

Fig. 17. Third-order limiter characteristic curve with input power at three frequencies in the passband. Unprimed operation is characterized by high output power and abrupt changes where additional plasma-shells activate, and primed operation shows lower output power and flatter slope.

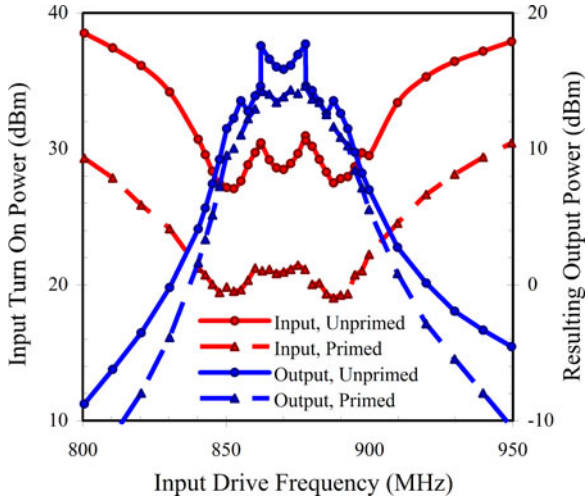

Fig. 18. Third-order filter-limiter turn-on power threshold versus drive frequency, with output power at each turn-on level. Priming reduces turn-on threshold power and eliminates the output power pedestal from unprimed operation.

in addition to the first. The transmission response is similar to the first-order case but with the added complexity of multiple plasma-shells that can activate independently.

The effect of additional on-state plasma-shells is clearly seen in Fig. 17, in which the limiter transfer characteristic is measured using the test setup in Fig. 9(c) at three frequencies: the lower band edge at 849 MHz, the band center at 870 MHz, and the midway at 860 MHz. The solid traces show passive "unprimed" operation where plasma-shells directly activate from incident power, and each frequency shows a unique characteristic curve with different slope, output level, and abrupt transitions where additional plasma-shells activate.

High output power and variable operation in the on-state are undesirable, so a method was devised to eliminate this behavior. Plasma-shells were "primed" by an external voltage source to a very low plasma density using external keep-alive electrodes consisting of thin wires in contact with each shell. Low-level glow discharge provides a source of free electrons to initiate plasma discharge, reducing turn-on threshold voltage and eliminating abrupt output power changes. This is a desirable alternative to traditional keep-alive electrodes that reduce operating lifetime of dc-coupled plasma devices, and avoid the use of radioactive materials [24]. Priming increased insertion loss by only 0.05 dB.

Reduced plasma-shell activation power is clearly demonstrated in Fig. 18 in which the input turn-on threshold power was recorded at each input drive frequency, along with resulting output power level. Priming reduced the average turn-on power in the passband from 29 to 20 dBm, and reduced resulting output power by 2 dB. Variation of turn-on and output power across the passband decreased by 1 dB, and the unprimed output power pedestal was eliminated.

Third-order filter-limiter maximum attenuation while operating in the limiter region was predicted by the Sonnet model, first for one on-state plasma-shell by setting R_g to the critical value; critical attenuation is 17.0 dB for the first resonator, 11.1 dB for the second, and 16.8 dB for the third. Critical attenuation for the entire filter was considered with all plasma-shells at the critical point, resulting in 52.5 dB. This prediction is useful because it occurs well beyond the capability of the test system where the highest measured attenuation at f_0 was 39.2 dB and was clearly operating in the limiter region with near-zero slope.

IV. Conclusion

This study demonstrated a combined narrowband filter and HPM plasma limiter device composed of a traditional microstrip bent hairpin filter with discrete plasma-shells across resonator ends. AC-coupled filter-limiter theory of operation and a plasma-shell equivalent circuit model were presented and validated with first-order filter-limiter measurements and EM simulation. A practical third-order filter-limiter demonstrated increased attenuation by cascading multiple resonators. Limiter performance was improved by priming the plasma-shells to a very low plasma density with an external voltage source without significantly increasing insertion loss.

AC-coupled plasma-shells have application beyond HPM limiters; they can be used at different frequencies, other filter topologies, and entirely different microwave structures at low and high power levels, operating passively from incident microwave power or actively from priming voltage sources. This study provides an introduction to the use of plasma-shells in microwave devices.

Acknowledgment

The authors gratefully acknowledge support from Dr. C. Bloebaum (Ex Director) and Dr. P. Collopy (Program Director) of the NSF EDI Program. The authors would like to thank Dr. A. Weisshaar (Ex Director, NSF ECCS) for his motivation, and J. D. Butcher and P. R. Cross for fabricating the devices.

REFERENCES

[1] M. G. Bäckström and K. G. Lövstrand, "Susceptibility of electronic systems to high-power microwaves: Summary of test experience," *IEEE Trans. Electromagn. Compat.*, vol. 46, no. 3, pp. 396–403, Aug. 2004.

[2] R. F. Bilotta, "Receiver protectors: A technology update," *Microw. J.*, vol. 40, no. 8, Aug. 1997.

[3] T. Nilsson, "Investigation of limiters for HPM and UWM front-door protection," M.S. thesis, Linköpings Univ., Linköpings, Sweden, 2006.

[4] B. M. Coaker, D. M. Dowthwaite, and N. E. Priestly, "High-power multifunction radar receiver protection," in *Proc. 3rd Eur. Radar Conf.*, Manchester, U.K., 2006.

[5] H. Goldie, "Radar receiver protector with auxiliary source of electron priming," U.S. Patent 4 245 197, Jan. 1981.

[6] L. T. Gritter, P. G. Krueger, C. J. Murphy, and R. M. Pap, "Method and apparatus for providing a carbon nanotube plasma limiter having a sub-ns response time," U.S. Patent 20080165466A1, Jan. 5, 2007.

[7] CPI Wireless Solutions, "Receiver protector technology," Beverly Microwave Division, Palo Alto, CA, USA. [Online]. Available: http://www.cpii.com/docs/related/4/RP%20Tech%20Art.pdf, Jul. 30, 2012.

[8] S. Balevičius, N. Zurauskienė, V. Stankevič, S. Keršulis, A. Abrutis, V. Plausinaitiene, and L. L. Altgilbers, "Fast protector against EMP using thin epitaxial and polycrystalline manganite films," *IEEE Electron Device Lett.*, vol. 32, no. 4, pp. 551–554, Apr. 2011.

[9] J. C. Booth, K. Leong, and S. A. Schima, "A superconducting microwave power limiter for high-performance receiver protection," *IEEE Trans. Microw. Theory Tech.*, vol. 1, pp. 139–142, Jun. 2004.

[10] A. A. Abidi, "The path to the software-defined radio receiver," *IEEE J. Solid-State Circuits*, vol. 42, no. 5, pp. 954–966, May 2007.

[11] M. P. Bachynski, "Electromagnetic wave penetration of reentry plasma sheaths," *Radio Sci. J. Research*, vol. 69D, no. 2, pp. 147–154, Feb. 1965.

[12] *R. P. Pipeline: That's Life*, CPI, Beverly Microwave Division, Beverly, MA, Sep. 1996. [Online]. Available: http://www.cpii.com/docs/related/4/TR%20Life.pdf

[13] E. G. Cristal and S. Frankel, "Hairpin-line and hybrid hairpin-line/half-wave parallel-coupled-line filters," *IEEE Trans. Microw. Theory Tech.*, vol. MTT-20, pp. 719–728, Nov. 1972.

[14] R. Levy, R. V. Snyder, and G. Matthaei, "Design of microwave filters," *IEEE Trans. Microw. Theory Tech.*, vol. 50, no. 3, pp. 783–793, Mar. 2002.

[15] J. Hong and M. J. Lancaster, "Couplings of microstrip square open-loop resonators for cross-coupled planar microwave filters," *IEEE Trans. Microw. Theory Tech.*, vol. 44, no. 12, pp. 2099–2109, Dec. 1996.

[16] R. J. Vidmar, "On the use of atmospheric pressure plasmas as electromagnetic reflectors and absorbers," *IEEE Trans. Plasma Sci.*, vol. 18, no. 4, pp. 733–741, Aug. 1990.

[17] Y. P. Raizer and J. E. Allen, *Gas Discharge Physics*. vol. 1, Berlin, Germany: Springer-Verlag, 1991, pp. 52–67.

[18] M. Lofgren, D. Anderson, H. Bonder, H. Hamnen, and M. Lisak, "Breakdown phenomena in microwave transmit-receive switches," *J. Appl. Phys.*, vol. 69, no. 4, pp. 1981–1992, Feb. 1991.

[19] F. M. Penning and C. C. Addink, "The starting potential of the glow discharge in neon-argon mixtures between large parallel plates," *Physica*, vol. 1, pp. 1007–1027, May 1934.

[20] D. L. Bitzer, H. G. Slottow, and R. H. Willson, "Gaseous display and memory apparatus," U.S. Patent 3 559 190, Jan. 1971.

[21] D. G. Swanson, "Narrow-band microwave filter design," *IEEE Microw. Mag.*, vol. 8, no. 5, pp. 105–114, Oct. 2007.

[22] Rogers Corp., "RO4000 series high frequency circuit materials," [Online]. Available: http://www.rogerscorp.com/documents/726/acm/RO4000-Laminates—Data-sheet.aspx, Nov. 1, 2012.

[23] Sonnet EM, (2012, Nov. 1). [Online]. Available: www.sonnetsoftware.com/products/sonnet-suites/

[24] H. Goldie, "Radioactive (tritium) ignitors for plasma limiters," *IEEE Trans. Electron Devices*, vol. 19, no. 8, pp. 917–928, Aug. 1972.

Lee W. Cross (S'11) received the B.S. and M.S. degrees in electrical engineering from The University of Toledo, Toledo, OH, USA, in 2002 and 2007, respectively, where he is currently working toward the Ph.D. degree with research in the area of microwave filter design.

He was with Imaging Systems Technology as Director of RF Research and is the principal investigator of research projects developing technology utilizing high-power RF and plasma devices.

Mohammad J. Almalkawi (M'12) received the B.Sc. degree in telecommunications engineering (Hons.) from Yarmouk University, Irbid, Jordan, the M.Sc. degree in electrical engineering from South Dakota School of Mines & Technology, SD, USA, and the Ph.D. degree in engineering from the University of Toledo, OH, USA, in 2007, 2009, and 2011, respectively.

In the summer of 2011, he was an Intern-RF Modeling Engineer with Freescale Semiconductor, Inc., Tempe, AZ, where he was involved in research on modeling RF/microwave components for the development of product-level models. In January 2012, he joined the Electrical Engineering and Computer Science Department, The University of Toledo, Toledo, OH, USA, as a Postdoctoral Research Associate and is currently a Research Assistant Professor. He has published more than 20 research papers in international journals and conferences. His current research interests include RF/microwave circuit design and modeling, UWB antennas, computational electromagnetics, and electromagnetic compatibility.

Dr. Almalkawi is currently a member of the Editorial Board of the *International Journal of RF and Microwave Computer-Aided Engineering*.

Vijay K. Devabhaktuni (SM'09) received the B.Eng. degree in electrical and electronics engineering and the M.Sc. degree in physics both from the Birla Institute of Technology and Science, Pilani, Rajasthan, India, in 1996, and the Ph.D. degree in electronics from Carleton University, Ottawa, ON, Canada, in 2003. He was awarded the Carleton University's senate medal at the Ph.D. level.

During 2003–2004, he held the Natural Sciences and Engineering Research Council of Canada (NSERC) postdoctoral fellowship and spent the tenure researching at the University of Calgary. In spring of 2005, he taught at Penn State Erie Behrend. During 2005–2008, he held the prestigious Canada Research Chair in Computer-Aided High-Frequency Modeling and Design at Concordia University, Montreal, Qubec, Canada. Since 2008, he has been an Associate Professor in the Electrical Engineering and Computer Science Department, The University of Toledo, Toledo, OH, USA. His research interests include applied electromagnetics, biomedical applications of wireless sensor networks, computer aided design, device modeling, image processing, infrastructure monitoring, neural networks, optimization methods, RF/microwave devices, and virtual reality applications. In these areas, he secured external funding close to $4M (sponsoring agencies include AFOSR, CFI, ODOT, NASA, NSERC, NSF, as well as industry). He coauthored more than 150 peer-reviewed papers, and is advising 11 M.S./Ph.D. students and 2 research faculties. He has won several teaching excellence awards in Canada and the USA.

Dr. Devabhaktuni currently serves as the Associate Editor of the *International Journal of RF and Microwave Computer-Aided Engineering* and as the Associate Editor of the IEEE MICROWAVE MAGAZINE. He is a registered member of the Association of Professional Engineers, Geologists, and Geophysicists of Alberta. He is a member of TC 36 on New Technologies and Applications for the IEEE International Microwave Symposium 2013.